Study on Photodegradation Activity of Fe3O4@SiO2@TiO2-Ce/rGO Magnetic Photocatalyst

Weiyan Cao
Qiqihaer University: Qiqihar University https://orcid.org/0000-0001-6187-8296
Liu Xijun (liuxijun2002@163.com)
Qiqihaer University: Qiqihar University
Wang Yuwei
Qiqihaer University: Qiqihar University
Zhang Yong
Qiqihaer University: Qiqihar University
Han Xianxin
Qiqihaer University: Qiqihar University
Fu Congzhi
Qiqihaer University: Qiqihar University

Nano Express

Keywords: Photocatalytic, magnetic, Graphene; Ce, TiO2

Posted Date: April 1st, 2021

DOI: https://doi.org/10.21203/rs.3.rs-338828/v1

COMMUNICATION

Study on photodegradation activity of Fe_3O_4@SiO_2@TiO_2-Ce/rGO magnetic photocatalyst

Received 00th January 20xx,
Accepted 00th January 20xx

DOI: 10.1039/x0xx00000x

Weiyan Cao[a] , Liu Xijun*[b] , Yuwei Wang[c] , Yong Zhang[d], Xianxin Han[e] and Congzhi Fu[f]

Abstract The magnetic core-shell Fe_3O_4@SiO_2@TiO_2-Ce/rGO composite nanomaterials were prepared by sol-gel method and hydrothermal method, composite photocatalyst doped with metal and loaded with graphene, the catalytic activity has been greatly improved. Under normal experimental conditions (pH = 7, [MB] = 10mg/L, magnetic composite photocatalyst concentration = 0.1g/50mL), Fe_3O_4@SiO_2@TiO_2-Ce/rGO nano-composites photocatalyst maximum degrade MB reaches 98.2% in 140 minutes.

Keywords: Photocatalytic; magnetic; Graphene; Ce; TiO_2.

1.Introduction

With the continuous advancement of the industrial revolution, the problem of water pollution has become increasingly serious. Polluted water sources seriously endanger human health, and it is extremely important to solve the problem of water pollution[1]. There are many types of pollutants in water sources, such as organic pollutants, inorganic pollutants, harmful metal ions, and harmful nitrogen oxide. Traditional sewage treatment methods are low in efficiency, high in cost, and selective to different pollutants. In particular, there are secondary pollution problems. Therefore, sewage treatment has not been well solved[2]. As early as 1972, Fujishima and Honda discovered that TiO_2 in photocells could be redoxed by water to release clean energy (H_2/O_2) when exposed to light[3]; in 1976, Carey et al. Used TiO_2 semiconductors to degrade organic pollutants[4]. Since then, photocatalytic oxidation has entered a stage of rapid development as a new water treatment technology.

TiO_2 photocatalytic degradation is the most suitable and available method for the treatment of organic compounds. The TiO_2 photocatalyst has the characteristics of good stability, low cost, strong catalytic activity, and is not harmful to the environment. The photocatalytic efficiency of nano titanium dioxide is related to crystal phase, particle size and specific surface area. Anatase has been demonstrated that anatase is the most stable and effective polymorph at nanoscale due to its relatively low surface energy [5-7]. However, due to the large band gap of TiO_2, high recombination rate of photogenerated carriers, and difficult to recycle characteristics, the application of TiO_2 in water treatment is limited. At present, a small amount of doping of TiO_2 with transition metal lanthanide series and metal actinide series metals can reduce the band gap width of TiO_2, make it also have photoresponse in the visible light region, thereby improving the utilization of sunlight[8]. Studies on doping of transition metals, including Ce, Co, Ni, etc., have been reported, the modification effect of Ce is better as compared to that of other transition metals[9-13]. In addition, TiO_2 photocatalyst makes their complete recovery from the wastewater difficult. This presents a major drawback to the application of the photocatalytic processes for treating wastewaters. Although many research groups have developed magnetic core-shell catalysts containing TiO_2 that can be quickly separated from sewage[14,15]. However, The magnetic core may be reduce the photocatalytic efficiency[16], To resolve this problem, SiO_2 can be applied as a barrier layer to form Fe_3O_4@SiO_2 which will not allow the interaction between the magnetic core and the TiO_2 coating[17-19]. Meanwhile, Graphene is a two-dimensional nanomaterial with high specific surface area and high conductivity[20,21], it can improve the migration efficiency of photogenerated carriers, Therefore, the recombination of photogenerated carriers can be effectively suppressed.

In this study, Fe_3O_4@SiO_2@TiO_2-Ce/ RGO core-shell nano photocatalyst was prepared by sol-gel method and hydrothermal method, the TiO_2 doped with rare earth metal Ce is loaded on graphene oxide to improve photocatalytic activity, and, Ce metal acts as an electron receiver to reduce electron-hole recombination, Graphene has good electrical conductivity and large specific surface area, It can increase the contact area between pollutants and the catalyst and improve the catalytic activity of the catalyst. The principle is shown in Figure 1.

[a] Qiqihar University Qiqihar Univ, Sch & Engn, Qiqihar 161006, Peoples R China. E-mil: 992257217@qq.com
*[b] Qiqihar University Qiqihar Univ, Sch & Engn, Qiqihar 161006, Peoples R China. E-mil: liuxijun2002@163.com（Corresponding Author）
[c] Qiqihar University Qiqihar Univ, Sch & Engn, Qiqihar 161006, Peoples R China. E-mil: ywwang@qqhru.edu.cn

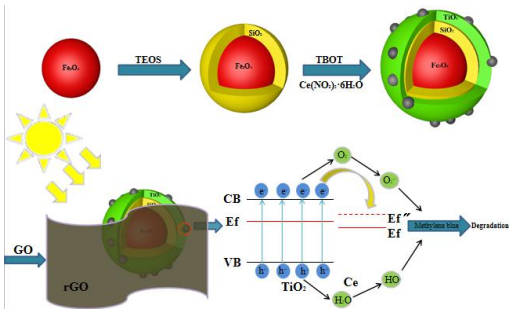

Figure 1. Fe_3O_4@SiO_2@TiO_2-Ce/rGO Principle of reaction

2. Experimental

2.1 Materials

Reagent: Fe_3O_4, Luoyang Haorun Information Technology Co. Ltd.; Graphene Oxide, Shenzhen Tuling Evolution Technology Ce. Ltd.; Tetrabutyl titanate (TBOT), Rhodamine B (RhB), Sodium dodecylbenzene sulfonate (SDBS), HNO_3, glacial acetic acid, $Ce(NO_3)_3 \cdot 6H_2O$, C_2H_5OH, Tianjin Komiou Chemical Reagent Ce, Ltd. All chemical reagents are of analytical grade, and them were used without further purification.

2.2 Synthesis of Fe_3O_4@SiO_2 nanoparticles

Weigh Fe_3O_4 (0.3g) into a 100mL beaker, and dilute HCl (50 mL, 0.1 mol L^{-1}) was added for sonication for 15min. Then, the Fe_3O_4 solid was magnetically separated and washed three times with deionized water. The magnetically separated Fe_3O_4 solid was put into a 250mL three-necked flask, and deionized water (18mL) and absolute ethanol (80mL) were added. Then, NH_3H_2O (2mL) and TEOS (0.6mL) was slowly added to the solution under stirring which continued for 12h at room temperature. The Fe_3O_4@SiO_2 were magnetically separated and washed three times with deionized water and absolute ethanol and dried at 60 ℃ under for 12h to obtain Fe_3O_4@SiO_2 powder.

2.3 Synthesis of Fe_3O_4@SiO_2@TiO_2-Ce nanoparticles

0.1g of $Ce(NO_3)_3$ was weighed into a 100 mL beaker, and then A solution was prepared by sequentially adding 1 mL of H_2O, 0.2 mL of HNO_3, and 20 mL of absolute ethanol. 0.2g of Fe_3O_4 was weighed in a 100 mL beaker, and 20 mL of absolute ethanol, 0.3mL of glacial acetic acid, and 8 mL of TEOT were gradually added, then mechanically stirred at room temperature for 30 min to prepare a B solution. The solution A was slowly added dropwise to the solution B, stirred well until a gel was formed, and aged at room temperature for 24h. After drying, it was calcined in an N_2 atmosphere for 2 h to obtain Fe_3O_4 @SiO_2 @TiO_2- Ce powder.

2.3 Synthesis of Fe_3O_4@SiO_2@TiO_2-Ce/rGO nanoparticles

0.08g of graphene oxide was dispersed in a mixture of deionized water and absolute ethanol, and ultrasonically dispersed for 1h. Then 0.15g SDBS and 0.2g Fe_3O_4@TiO_2-Ce were added in sequence, and ultrasonic dispersion was continued for 1h. The solution was transferred to a polytetrafluoroethylene autoclave and reacted in an oven at 120℃ for 3h. The product was washed three times with anhydrous ethanol and deionized water, respectively, and then dried at 60℃ for 24h to obtain Fe_3O_4@SiO_2@TiO_2-Ce/rGO photocatalyst.

3. Results and discussion

3.1 XRD analysis

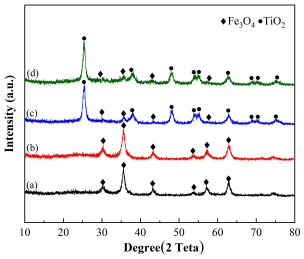

Figure 2. XRD spectrum of Fe_3O_4(a) 、 Fe_3O_4@SiO_2(b) 、 Fe_3O_4@SiO_2@TiO_2-Ce(c) and Fe_3O_4@SiO_2@TiO_2-Ce/rGO(d)

As shown in figure 2 (a), characteristic diffraction peaks appear at 30.0, 35.3, 43.0, 53.5, 56.9 and 62.8, corresponding to (220), (311), (400), (422), (511) and (440) crystal planes (JCPDS No.26 - 1136), they belong to characteristic diffraction peak of Fe_3O_4 Comparing Fig. 2 (a) and (b), It is not difficult to find that there is no obvious change between Fe_3O_4 and Fe_3O_4@SiO_2. This may be because the SiO_2 coating is amorphous, so no new diffraction peaks. Figure 2 (c)Fe_3O_4@SiO_2@TiO_2-Ce and (d)Fe_3O_4@SiO_2@TiO_2-Ce/rGO have similar characteristic peaks, In addition to the characteristic diffraction peaks of Fe_3O_4, New characteristic diffraction peaks appeared at 25.8, 37.8, 48.0, 53.8, 55.0, 62.1, 68.8, 70.3 and 75.0, corresponding to (101), (004), (200), (105), (211), (213), (116), (220) and (215) crystal planes (JCPDS number 21-1272). It shows that the introduced TiO_2 is mainly anatase phase, As shown in Figure 2(c, d), no characteristic diffraction peaks of rGO and Ce were found, this may be because the amount of Ce and GO is too small and the detection is not obvious.

3.2 SEM images analysis

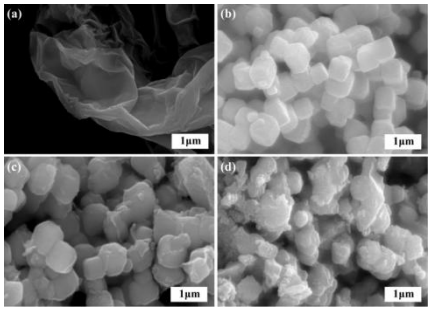

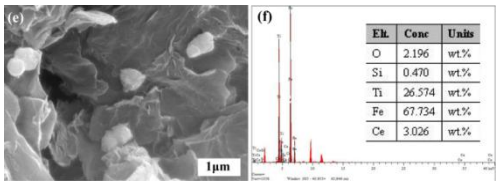

Figure 3. SEM images of rGO(a)、 Fe_3O_4(b)、 Fe_3O_4@SiO_2(c)、 Fe_3O_4@SiO_2@TiO_2-Ce(d)、 Fe_3O_4@SiO_2@TiO_2-Ce/rGO(e) and EDs of Fe_3O_4@SiO_2@TiO_2-Ce(f)

The typical lamellar structure of GO can be clearly seen in Figure 3a; Figure 3b shows that the Fe_3O_4 particles have a tetragonal structure,The particle size is about 400nn and evenly distributed; Figure 3c can clearly show that the Fe_3O_4 surface becomes smooth; The edges and corners are no longer clear, at the same time the particle size has increased, indicating that SiO_2 has been successfully wrapped on the surface of Fe_3O_4; Figure 3d shows that the surface becomes rough with granular substances, The EDS spectrum shows that the Ce content is 3%, indicating that Ce metal has been successfully doped on the surface of TiO_2. Figure 3e shows that Fe3O4@SiO2@TiO2-Ce has been successfully loaded on rGO. .

3.3 TEM images analysis

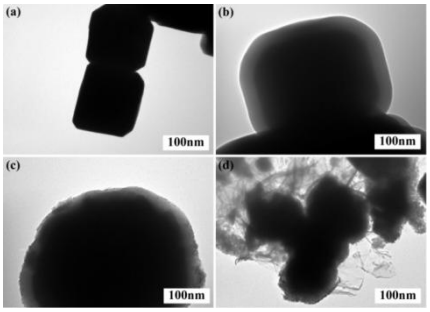

Figure 4. TEM images of Fe_3O_4(a) 、 Fe_3O_4@SiO_2(b) 、 Fe_3O_4@SiO_2@TiO_2-Ce(c) and Fe_3O_4@SiO_2@TiO_2-Ce/rGO(d)

In order to further clarify the morphology of the sample, Research group had performed TEM image analysis on Fe_3O_4, Fe_3O_4@SiO_2, Fe_3O_4@SiO_2@TiO_2-Ce and Fe_3O_4@SiO_2@TiO_2-Ce/rGO. Figure 4a shows the tetragonal configuration of Fe_3O_4 more clearly; Figure 4b shows that a translucent part is formed on the surface of Fe_3O_4, It shows that Fe_3O_4 and SiO_2 form a core-shell structure; Figure 4c shows that there are more obvious particles on the outer surface of the particles, It further proves that Ce particles have been successfully doped on the surface of Fe_3O_4@SiO_2@TiO_2, Figure 4d shows that Fe_3O_4@SiO_2@TiO_2-Ce is tightly supported on the surface of rGO, One step further confirmed the successful preparation of Fe_3O_4@SiO_2@TiO_2-Ce/rGO composite nanoparticles in this experiment.

3.4 FT-IR analysis

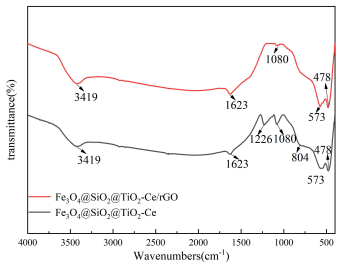

Figure 5. FT-IR spectra of Fe_3O_4@SiO_2@TiO_2–Ce and Fe_3O_4@SiO_2@TiO_2–Ce/rGO

FT-IR analysis was used to study the bonding interactions in the fabricated Fe_3O_4@SiO_2@TiO_2–Ce and Fe_3O_4@SiO_2@TiO_2–Ce/rGO nano-photocatalyst. The wide band at 3419 cm-1 is attributed to the tensile vibration of surface water or hydroxyl (-OH) groups； The characteristic peak of Si-O-Si corresponds to 1080cm^{-1} (antisymmetric stretching vibration); Fe-O characteristic peak is at 573cm^{-1} (asymmetric stretching vibration)[22]; The characteristic peak of Ti-O-Ti is at 478 cm^{-1} (stretching vibration); 807cm^{-1} (symmetrical stretch) is Ti-O-Si[17]; C = C (double bond stretching vibration) zone is at 1623cm^{-1}[23]. The two curves have not changed significantly, There is an obvious C-C impurity peak at 1226cm^{-1} in Fe_3O_4@SiO_2@TiO_2-Ce, With the addition of graphene, the peak at C=C in Fe_3O_4@SiO_2@TiO_2–Ce/rGO is more obvious.

3.5 UV-Vis DRS analysis

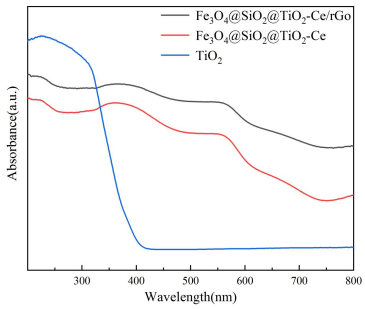

Figure 6. UV-Vis DRS spectra of and Fe_3O_4@SiO_2@TiO_2–Ce/rGO, Fe_3O_4@SiO_2@TiO_2–Ce and TiO_2

It can be seen from the ultraviolet-visible diffuse reflectance spectrum of the catalyst (in Figure 6). Pure TiO_2 samples have strong absorption in the ultraviolet region, But there is almost no absorption in the visible light region, The absorption intensity of the nano-photocatalyst doped with Ce is significantly enhanced under visible light, Redshift of the absorbing boundary. This shows that Ce doping can expand the response range of TiO_2 in the visible light region. The nano-photocatalyst loaded with rGO further improves the absorption performance of the catalyst under visible light. So, it improves the catalytic activity of the photocatalyst.

3.6 N_2 adsorption–desorption analysis analysis

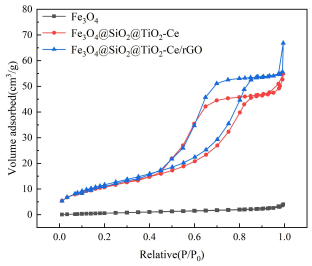

Figure7. Nitrogen adsorption–desorption isotherms of the Fe_3O_4, Fe_3O_4@SiO_2@TiO_2-Ce, and Fe_3O_4@SiO_2@TiO_2-Ce/rGO

The adsorption performance of photocatalyst was characterized by N_2 physical adsorption experiment, the corresponding N_2 adsorption-desorption isotherm is shown in Figure 7. It can be seen that the samples Fe_3O_4@SiO_2@TiO_2-Ce， Fe_3O_4@SiO_2@TiO_2-Ce /rGO show the shape of type IV isothermal curve that they are mesoporous structures, electron microscopy test showed that the particle size was about 40nm. It was confirmed by previous electron microscopy tests. The test results show that the specific surface areas of Fe_3O_4, Fe_3O_4@SiO_2@TiO_2-Ce and Fe_3O_4@SiO_2@TiO_2-Ce/rGO are 3.7660 m^2/g, 40.6405 m^2/g and 46.9017 m^2/g, The increase in specific surface area is conducive to the adsorption of pollutants, promote the photocatalytic degradation of pollutants.

3.7 EIS analysis

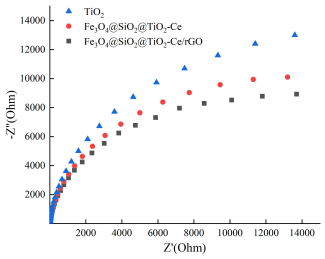

Figure 8. EIS of the TiO_2, Fe_3O_4@SiO_2@TiO_2-Ce, and Fe_3O_4@SiO_2@TiO_2-Ce/rGO

EIS spectrum is a test method used to characterize charge transfer. The smaller the curve radius, the smaller the resistance.The Nyquist curve in Figure 9 has the largest radius of TiO_2, The second is Fe_3O_4@SiO_2@TiO_2-Ce, the smallest is Fe_3O_4@SiO_2@TiO_2-Ce/rGO nanocomposite. It shows that Fe_3O_4@SiO_2@TiO_2-Ce/rGO nanocomposite has the highest charge transfer efficiency. This is due to the large π-bond structure of the loaded graphene, which promotes photogenerated electron transfer, graphene is also an excellent electron acceptor. Thereby reducing the recombination with holes, It is consistent with the UV test.

3.8 PL analysis

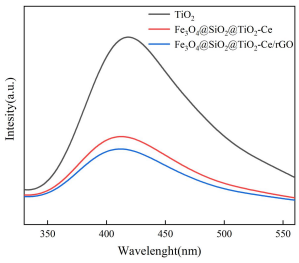

Figure 9. PL spectra of nano-photocatalyst samples.

The recombination of photo-generated carriers will reduce the activity of TiO_2 photocatalyst, Therefore PL analysis is used to measure the luminescence intensity of the fluorescence generated by the recombination of photo-generated carriers. Figure 9 above, It can be clearly seen that the fluorescence intensity of pure TiO_2, Fe_3O_4@SiO_2@TiO_2-Ce, Fe_3O_4@SiO_2@TiO_2-Ce/rGO gradually decreases. It shows that doping Ce and loading rGO reduces the recombination efficiency of photogenerated carriers. This is consistent with the EIS results. Therefore, the photocatalytic activity is improved.

3.9 Photocatalytic properties analysis

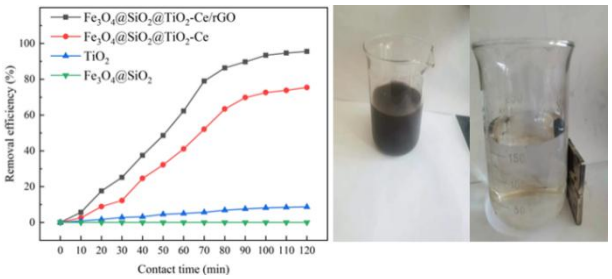

Figure 10.The catalytic activity of Fe_3O_4@SiO_2, TiO_2, Fe_3O_4@ SiO_2@TiO_2-Ce and Fe_3O_4@SiO_2@TiO_2-Ce/ rGO and the magnetic test chart of Fe_3O_4@SiO_2@TiO_2-Ce/rGO

The photocatalytic activity of the sample was studied by the photodegradation rate of MB under visible light irradiation.The absorbance of MB after degradation was measured with ultraviolet-visible-near-infrared spectrophotometer. The degradation efficiency of the photocatalyst increases with time.The photocatalytic activity of Fe_3O_4@SiO_2 is 0; the photocatalytic activity of TiO_2 is very low, and the degradation rate is 8.7%; The photocatalytic activity of Fe_3O_4@SiO_2@TiO_2-Ce nanocomposite material obtained after metal Ce doping has been greatly improved, and the degradation rate is 75.4%; Fe_3O_4@SiO_2@TiO_2-Ce/rGO nanocomposite is 98.2%. It shows that the supported graphene plays a great role in improving the photocatalytic activity of the photocatalyst. This is because the excitation TiO_2 conduction band electrons can be transferred to the

graphene sheet, This prevents photogenerated electrons from recombining with holes， it is consistent with PL test results；The UV-Vis DRS test also proved that the modified TiO_2 photocatalyst has been greatly improved in the visible light absorption region；The EIS test results are consistent with UV-Vis DRS test and PL test. Therefore, the photocatalytic activity is improved. As shown in the right picture of Figure 10. Fe_3O_4@SiO_2@TiO_2-Ce/rGO nanocomposite materials can be easily aggregated by magnetic substances, So as to achieve the purpose of convenient recycling.

4. Conclusions

Therefore, the prepared by sol-gel method and hydrothermal method. The morphology and structure were characterized by TEM, SEM, xrd and FT-IR, and Performance tests for UV-Vis DRS, PL, N2 gas adsorption, EIS, etc. All proved that the prepared Fe_3O_4@SiO_2@TiO_2-Ce/rGO nanocomposite has high catalytic activity. In addition, the catalytic activity of TiO_2 photocatalyst by doped metal cerium and supported reduced graphene oxide has been greatly improved. There are broad application prospects in the treatment of factory wastewater in the future.

Conflicts of interest

There are no conflicts to declare

Availability of data and material

The datasets supporting the conclusions of this article are included within the article.

Funding

The authors received no specifc funding for this work.

Authors' contributions

LX and WY guided the experiments and test process and revised the paper. CW designed, conducted the experiments and written the manuscripts. ZY and HXX tested. FC analyzed the data. All authors discussed the results and commented on the manuscript. All authors read and approved the fnal manuscript.

Acknowledgements

The authors greatly acknowledge the Qiqihaer University analysis and testing Center for the measurement assistance.

Notes and references

1 J. J. Yuan, Y. L. Lu, C. C. Wang, X. H. Cao, C. C. Chen, H. T. Cui, M. Zhang, C. Wang, X. Q. Li, A. C. Johnson, A. J. Sweetnnan and D. Du, Ecology of industrial pollution in China, Ecosystem Health And Sustainability, 2020, 6, 1-17.

2 B. Prasad, C. Ghosh, A. Chakraborty, N. Bandyopadhyay and R. K. Ray, Desalination, 2011, 274, 105-112.

3 A. Fujishima and K. Honda. Electrochemical Photosynthesis Of Water At A Semiconductor Electrode, Nature, 1972, **238**, 37-38.

4 J. H. Carey, J. Lawrence and H. M. Tosine, Photodechlorination of PCBS in Presence of Titanium Dioxide in Aqueous Suspensions, Bulletin of Environmental Contamination and Toxicology, 1976, **16**, 697-701.

5 K. J. Lin, J. Qian, Z. H. Zhao, G. L. Wu and H. J. Wu, Synthesis of a Carbon-Loaded $Bi_2O_2CO_3$/TiO_2 Photocatalyst with Improved Photocatalytic Degradation of Methyl Orange Dye, Journal Of Nanoscience And Nanotechnology, 2020, **20**, 7653-7658.

6 F. S. Han, L. Y. Zhu, Z. X. Huang and Z. H. Zhou, Photoinduced Superhydrophilicity of Anatase TiO_2 Surface Uncovered by First-Principles Molecular Dynamics, Journal of Physical Chemistry Letters, 2020, **11**, 7590-7593.

7 Y. S. Cho, Y. H. Lee and J. K. Park, Fabrication of Silica Microspheres Containing TiO_2 or Aluminum Zinc Oxide Nanoparticles via Self-Assembly: Application in Water Purification, Journal Of Nanoscience And Nanotechnology, 2020, **20**, 6738-6746.

8 Y. Y. Li, J. G. Wang, X. R. Liu, C. Shen, K. Y. Xie and B. Q. Wei, Au/TiO_2 hollow spheres with synergistic effect of plasmonic enhancement and light scattering for improved dye-sensitized solar cells, ACS Appl Mater. Interfaces, 2017, **9**, 31691-31698.

9 C. Z. Fu, X. J. Liu and Y. W. Wang, Synthesis and Characterization of Fe_3O_4@TiO_2-Ni/rGO Magnetic Photocatalyst, New Journal Chemistry, 2020, **44**, 5755-5761.

10 Mojtaba Rostami, Photodecomposition and adsorption of hazardous organic pollutants by Ce-doped ZnO@Ce-doped TiO_2-N/S-dual doped RGO ternary nano-composites photocatalyst for water remediation, Journal of Molecular Structure, 2019, **1185**, 191-199.

11 J. W. Hou, J. Y. Zhou, Y. F. Liu, Y. Yan, S. X. Zheng and Q. Y. Wang, Constructing Ag_2O nanoparticle nanoparticle modified TiO_2 nanotube arrays for enhanced photocatalytic performances, Journal Of Alloys And Compounds, 2020, **849**. https://doi.org/10.1016/j.jallcom.2020.156493.

12 D. D. Wang, Q. J. Li, W. Miao, Y. Liu, N. J. Du and S. Mao, One-pot synthesis of ultrafine NiO loaded and Ti^{3+} in-situ doped TiO_2 induced by cyclodextrin for efficient visible-light photodegradation of hydrophobic pollutants, Chemical Engineering Journal, 2020, **402**, https://doi.org/10.1016/j.cej.2020.126211

13 W. C. Li, L. K. Xie, L. X. Zhou, O. L. Josias, C. Li and X. J. Chai, A systemic study on Gd, Fe and N co-doped TiO_2 nanomaterials for enhanced photocatalytic activity under visible light irradiation, 2020, **46**, 24744-24752.

14 M. Shen, S. Q. Chen, W. P. Jia, G. D. Fan, Y. X. Jin and H. D. Liang, Highly efficient and porous TiO_2-coated Ag@Fe_3O_4@C-Aumicrospheres for degradation of organic pollutants, Journal Of Nanoparticle Research, 2016, **18**, doi:10.1007/s11051-016-3655-z.

15 Q. L. Hu, L. S. Wang, N. N. Yu, Z. F. Zhang, X. Zheng and X. M. Hu, Preparation of Fe_3O_4@C@TiO_2 and its application for oxytetracycline hydrochloride adsorption, Rare Metals, 2020, **39**, 1333-1340.

16 J. Q. Ma, S. B. Guo, X. H. Guo and H. G. Ge, Liquid-phase deposition of TiO_2 nanoparticles on core–shell Fe_3O_4@SiO_2 spheres: preparation, characterization and photocatalytic activity, Journal Of Nanoparticle Research, 2015, **17** , 10.1007/s11051-015-3107-1.

17 N. Esfandiaria, M. Kashefia, S. Afsharnezhad and M. mirjalili, nisght into enhanced visible light photocatalytic activity of Fe_3O_4–SiO_2–TiO_2 core-multishell nanoparticles on the elimination of Escherichia coli, Materials Chemistry and Physics, 2020, **244**, https://doi.org/10.1016/j.matchemphys.2020.122633

18 M. Mokhtarifar, R. Kaveh, M. Bagherzadeh and M. V. Diamanti, Heterostructured TiO_2/SiO_2/Fe_2O_3/rGO coating with visible light- induced self-cleaning properties for metallic artifacts, Acs Applied Materials & Interfaces, 2020, **12**, 29671-29683.

19 B. Dabirvaziri, M. H. Givianrad, I. Sourinejad, A. M. Moradi and P. G. Mostafavi, A simple and effective synthesis of magnetic γ-Fe_2O_3@SiO_2@TiO_2–Ag microspheres as a recyclable photocatalyst: dye degradation and antibacterial potential, Journal of Environmental Health Science and Engineering, 2019, **17**, 949-960.

20 P. Gupta, S. Rajkumar, P. Gopinath, Development of Sunlight-Driven Reduced Graphene Oxide (rGO)/CeO_2-CuO Nanofibrous Photocatalyst for Efficient Removal of Organic Dyes, Journal of Nanoscience and Nanotechnology, 2020, **20**, 7480-7494.

21 Y. H. Nien, H. H. Hsun, G. M. Hu, M. Rangasamy, Z. R. Yong, H. H. Chen, P. Y. Kuo, J. C. Chou, C. H. Lai, C. H. Kuo, C. C. Ko and J. X. Chang, Study of Novel Dye-Sensitized Solar Cells With Modified Photoelectrode by ZrO_2 and rGO Doped TiO_2 Composite Nanofibers, 2020, **69**, 3660-3666.

22 R. Khalifeh, V. Naseri and M. Rajabzadeh, Synthesis of Imidazolium-Based Ionic Liquid on Modified Magnetic Nanoparticles for Application in One-Pot Synthesis of Trisubstituted Imidazoles, Chemistryselect, 2020, **5**, 11453-11462.

23 C. Z. Fu, X. J. Liu, Y. W. Wang, L. Li and Z. H. Zhang,Preparation and Characterization of Fe_3O_4@SiO_2@TiO_2-Co/rGO Magnetic Visible Light Photocatalyst for Water Treatment, RSC Advances, 2019, **9**, 20256-20265.

Figures

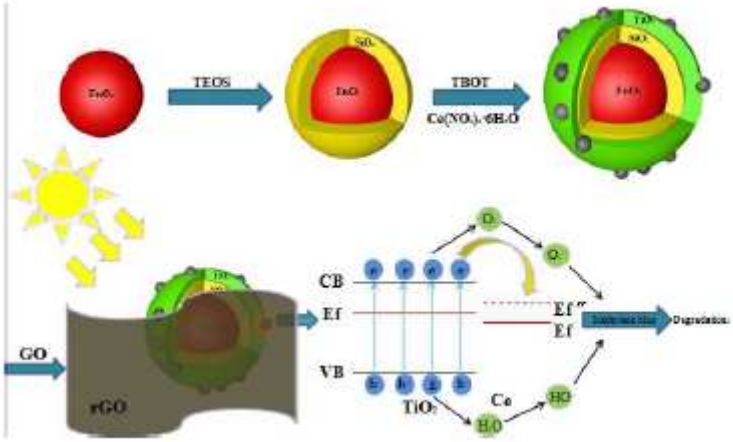

Figure 1

See the Manuscript Files section for the complete figure caption.

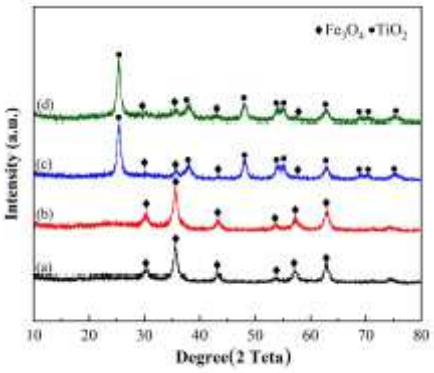

Figure 2

See the Manuscript Files section for the complete figure caption.

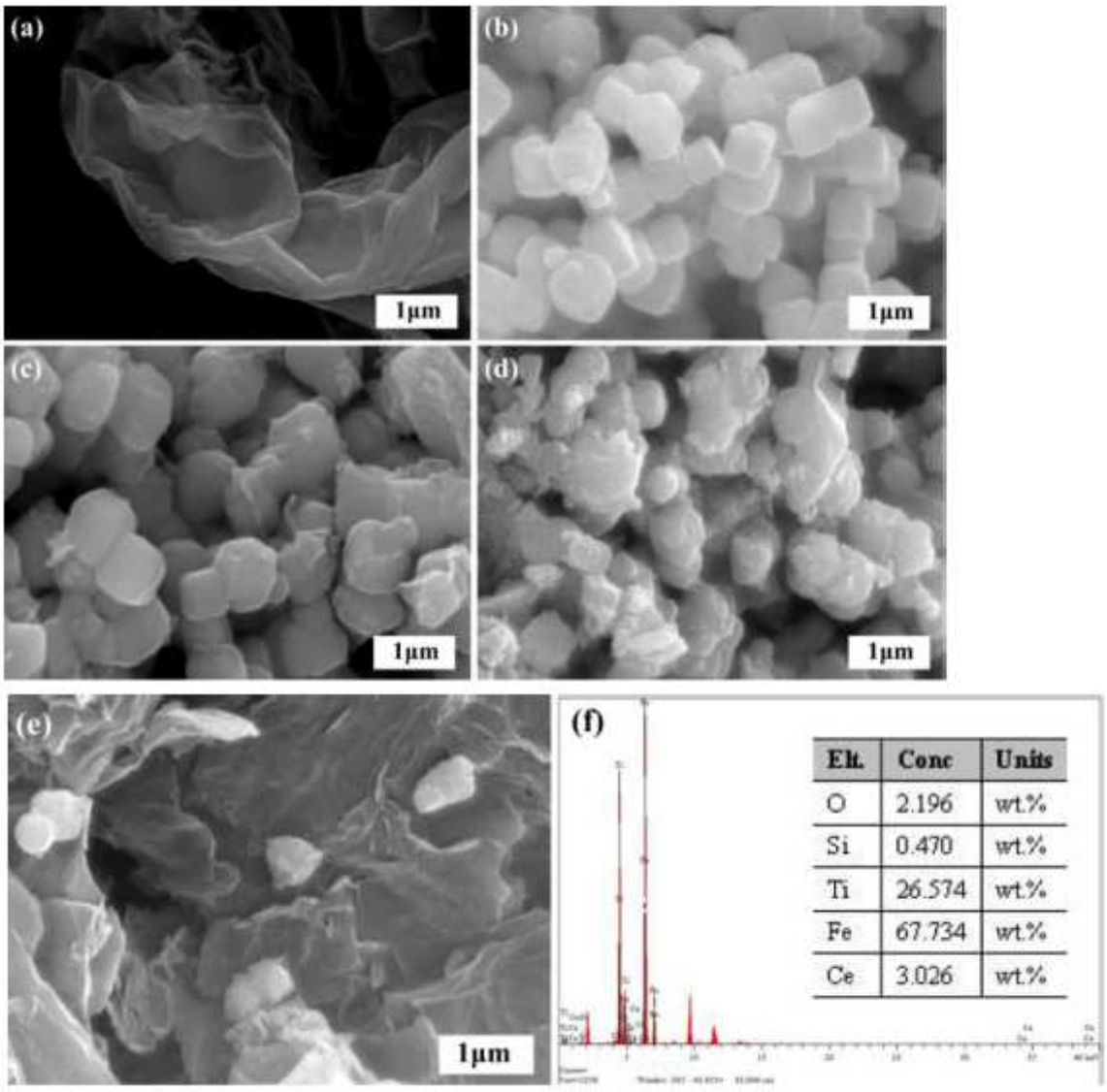

Figure 3

See the Manuscript Files section for the complete figure caption.

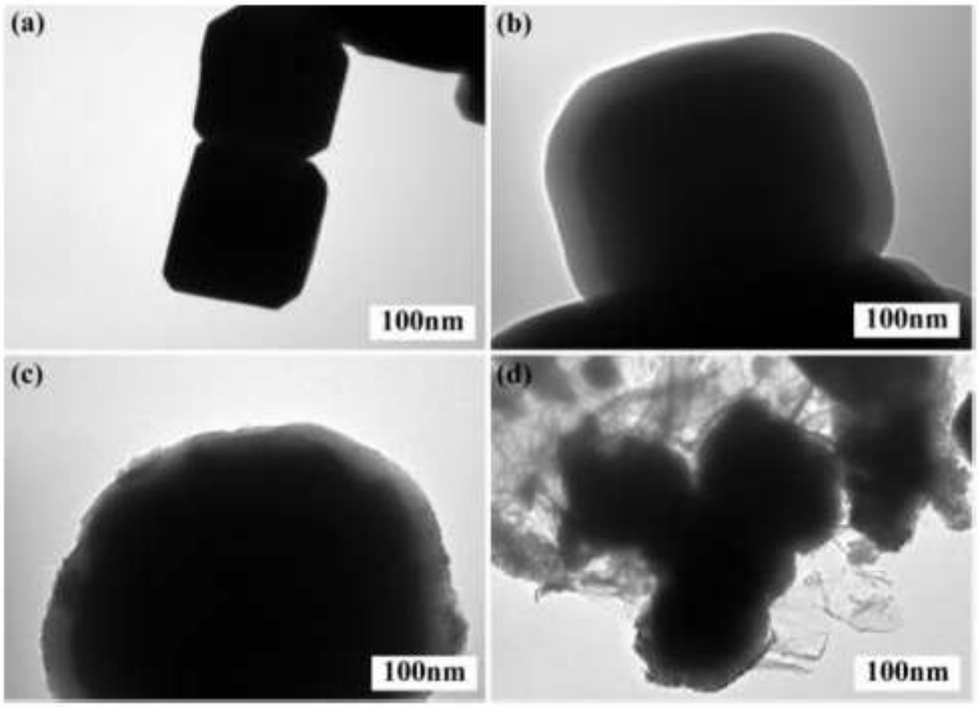

Figure 4

See the Manuscript Files section for the complete figure caption.

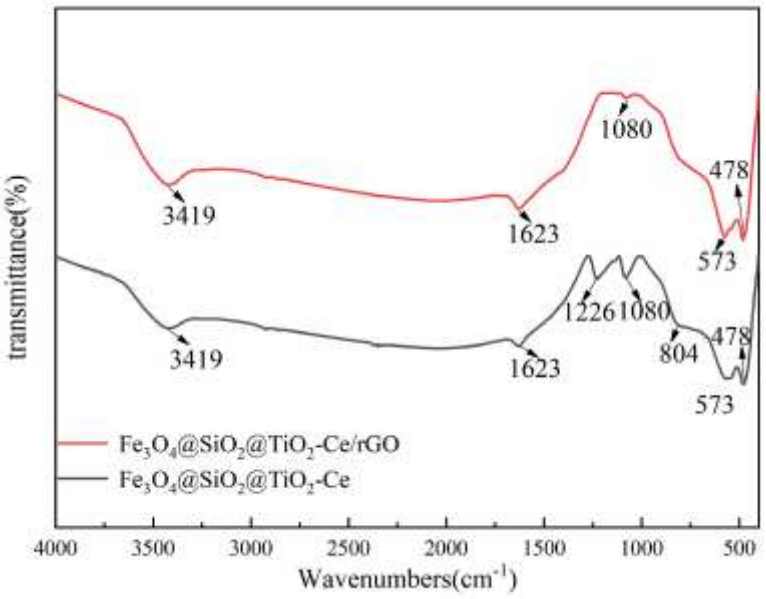

Figure 5

See the Manuscript Files section for the complete figure caption.

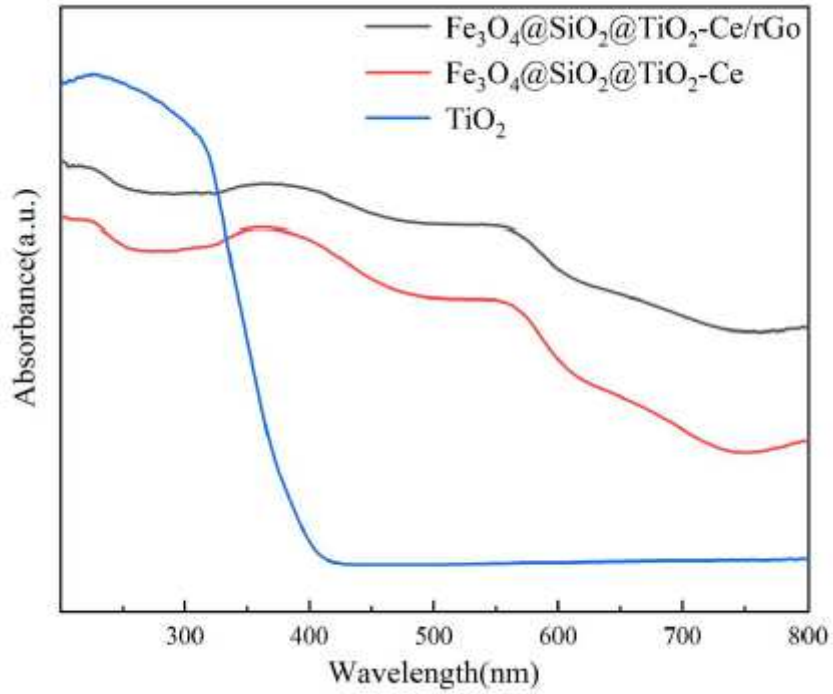

Figure 6

See the Manuscript Files section for the complete figure caption.

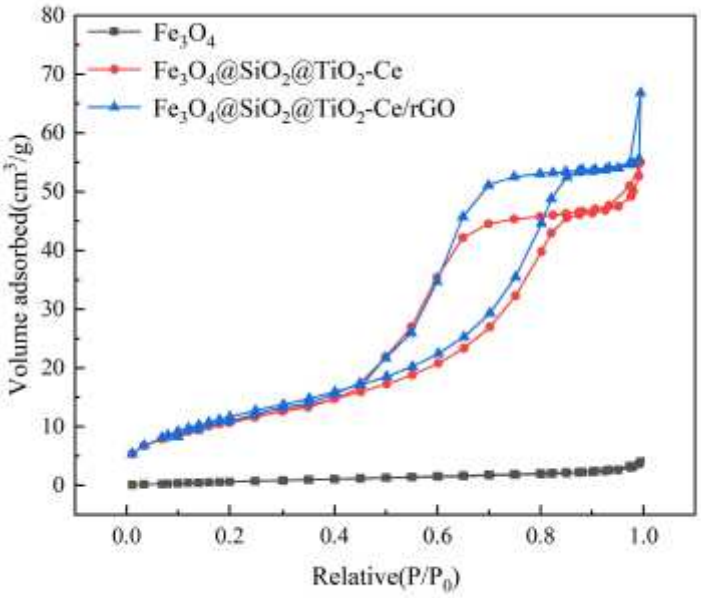

Figure 7

See the Manuscript Files section for the complete figure caption.

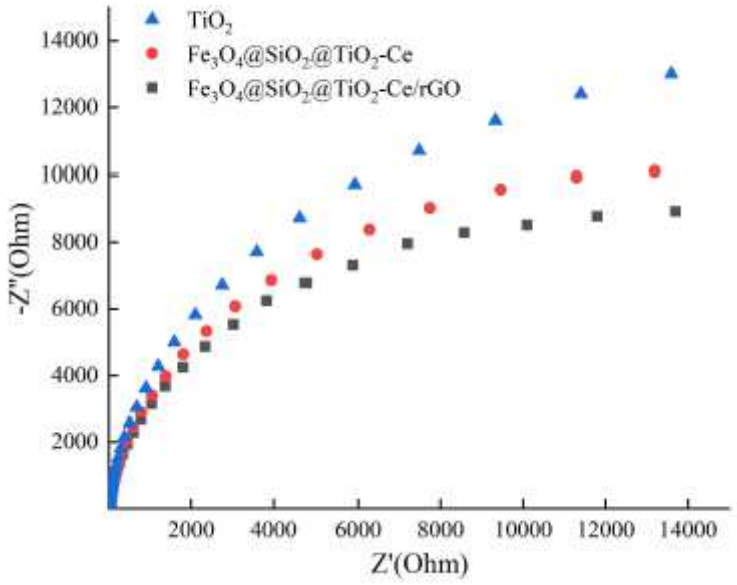

Figure 8

See the Manuscript Files section for the complete figure caption.

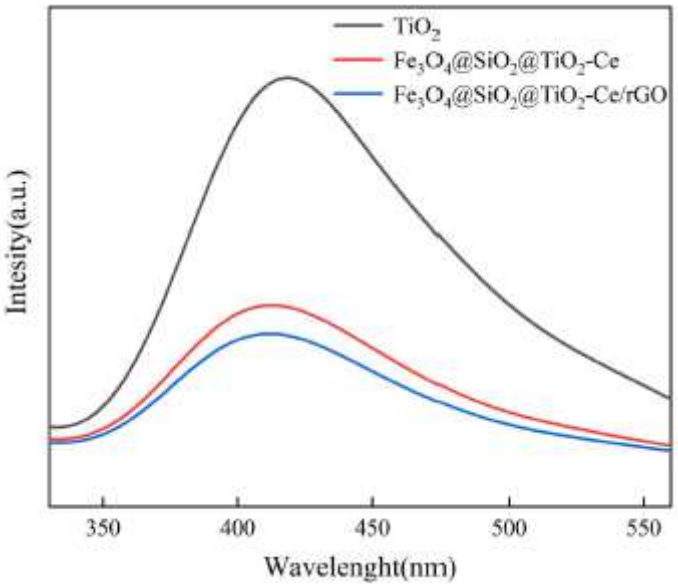

Figure 9

See the Manuscript Files section for the complete figure caption.

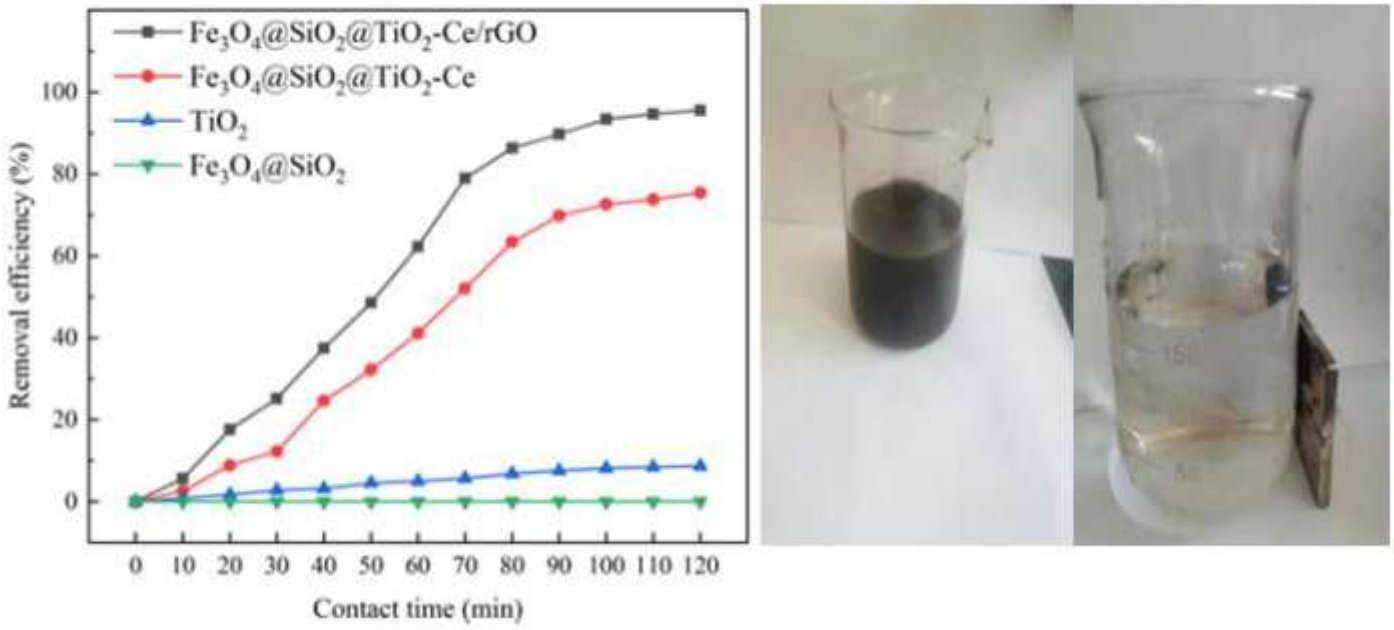

Figure 10

See the Manuscript Files section for the complete figure caption.